FABRICATION AND MASS ATTENUATION COEFFICIENT OF BIOPLASTIC *RHIZOPHORA SPP. PARTICLEBOARD*

by

LEILA GHASEMI

Thesis submitted in fulfillment of the requirements
for the degree of
Master of Science (Medical Physics)

UNIVERSITI SAINS MALAYSIA

February 2013

To my beloved parents

ACKNOWLEDGEMENT

Praises to Allah the Lord of the universe that has given me the strength, perseverance and intention to go through and complete my study.

I wish to express my sincere appreciation to my main supervisor Prof. Dr**.** Mohamad Suhaimi Bin Jaafar who was abundantly helpful and offered valuable assistance, support, guidance, critics and friendship.

I am heartily thankful to my co-supervisor, Assoc. Prof. Dr. Sabar Bauk who gave me valuable guidelines, helpful tip when I encountered problems. He was kind hearted, patient and a good listener.

My gratefulness also went to Prof. Dr. Rokiah Hashim, my second co-supervisor, for her guidance, advices and motivation. Without their continued support and interest, this thesis would not have been the same as presented here.

I would also like to express my sincere thanks to Dr. Mohammad Wasef Marashdeh for his great – by all means – guidance and assistance.

I owe my deepest gratitude to my beloved family, for their faith in me, their understanding and endless love and allowing me to be as ambitious as I wanted. This thesis would not have been possible without all sacrifices that my lovely family has done to enable me to complete my study. No word can describe my love to them.

TABLE OF CONTENTS

ACKNOWLEDGEMENTS ii

TABLE OF CONTENTS iii

LIST OF TABLES vii

LIST OF FIGURES viii

LIST OF APPENDICES xi

LIST OF SYMBOLS AND ABBREVIATIONS xii

ABSTRAK xv

ABSTRACT xvi

CHAPTER 1 INTRODUCTION 1

1.1 Background 1

1.2 Statement of Problems 2

1.3 Objectives of Research 3

1.4 Scope of Research 4

1.5 Outline of the Thesis 4

CHAPTER 2 LITERATURE REVIEW and THEORY 5

2.1 Linear Attenuation Coefficient 5

2.2 Mass Attenuation Coefficient 6

2.3 Interaction of Photon with Matter 7

2.3.1 Coherent Scattering 7

2.3.2 Photoelectric Effect 8

2.3.3 Compton Scattering 12

2.3.4 Pair Production 14

2.4 X-ray Fluorescence 15

2.4.1 Sources of X-ray Fluorescence (XRF) 16

2.5 Pulse Height Analyzers 17

2.6 Energy Resolution 18

2.7 Error Analysis 20

2.8 Phantom 22

2.9 Study on Mangrove Wood *Rhizophora spp*. Phantom 23

CHAPTER 3 MATERIALS and METHODS 28

3.1 Particleboard Fabrication 28

3.1.1 Adhesive Consideration 29

3.1.2 Polylactic Acid 30

3.1.3 Particle Preparation 32

3.1.4 Determination of the Moisture Content of *Rhizophora spp.* Particles 34

3.1.5 *Rhizophora spp*. Particleboard Fabrication 35

3.1.6 Preparation of *Rhizophora spp*. Particles with Different Resin Treatment Level 35

3.1.7 Preparation of Samples for Characterization tests 40

3.2 Mechanical and Physical Properties 40

3.2.1 Geometrical Density Measurement 40

3.2.2 Internal Bond (IB) Strength 41

3.2.3 Water Absorption 42

3.2.4 Thickness Swelling 43

3.2.5 Surface Morphology 43

3.3 Experiment Set up to Determine the Mass Attenuation of Fabricated *Rhizophora spp.* Particleboard 45

3.3.1 Low Energy Germanium Detector (LEGe) 45

3.3.2 Cryostat 46

3.3.3 MCA Measurement System 48

3.3.4 Excitation Source 48

3.4 Detection System 49

3.4.1 Detector Calibration 49

3.4.2 Energy Calibration 50

3.4.2.1 ^{241}Am Calibration 50

3.4.2.2 Pure Metal Plates 51

3.5 Measurement of the Linear Attenuation Coefficient and the Mass Attenuation Coefficient of BioPlastic *Rhizophora spp.* Particleboard Samples 52

CHAPTER 4 RESULTS AND DISCUSSION 55

4.1 Density of BioPlastic *Rhizophora spp.* Particleboard Samples 55

4.2 Internal Bond (IB) Strength 58

4.3 Water Absorption (WA) and Thickness Swelling (TS) 61

4.4 Microstructure Analysis 62

4.5 Energy Calibration 64

4.5.1 Radioactive Source Americium-241 (^{241}Am) Calibration 64

4.5.2 Pure Metal plates 66

4.5.3 Aluminum Measurement 67

4.6 Mass Attenuation Coefficient 68

CHAPTER 5 CONCLUSION 76

5.1 Conclusion 76

5.2 Recommendation 78

REFERENCES 79

APPENDICES 86

LIST OF TABLES

Table 3.1	The photon energies emitted from ^{241}Am	50
Table 4.1 (a)	Thickness, length and width of the particleboard with 10% PLA resin	56
Table 4.1 (b)	Volume, mass, density of the particleboard with 10% PLA resin.	56
Table 4.2	Comparison of density of fabricated *Rhizophora spp*. particleboards	58
Table 4.3	Comparison of internal bond strength (IB) of each bioplastic *Rhizophora spp*. particle board.	60
Table 4.4	Energy calibration for the Germanium Detector.	65
Table 4.5	Channel number corresponding to the energy of XRF from different metal plates.	66
Table 4.6 (a)	Measured linear and mass attenuation coefficients of bioplastic *Rhizophora spp*. particle board base on the K_α peaks of the characteristic X-ray of the metal targets	69
Table 4.6 (b)	Measured linear and mass attenuation coefficients of bioplastic *Rhizophora spp*. particle board base on the K_β peaks of the characteristic X-ray of the metal targets	69
Table 4.7	The χ^2 – test of mass attenuation coefficient of bioplastic *Rhizophora spp*. particleboards samples to XCOM calculated Breast 1.	72
Table 4.8	The χ^2 – test of mass attenuation coefficient of bioplastic *Rhizophora spp*. particleboards samples to XCOM calculated Breast 2.	73
Table 4.9	The χ^2 – test of mass attenuation coefficient of bioplastic *Rhizophora spp*. particleboards samples to XCOM calculated Breast 3.	73

LIST OF FIGURES

Figure 2.1	Coherent scattering. A photon with energy *hv* interacts with a K-shell electron. This scattered X-ray has the same wavelength ($\lambda = \lambda'$) as the incident beam	8
Figure 2.2	Schematic diagram of photoelectric effect. A photon with energy *hv* interacts with a K-shell electron. The photon is absorbed completely and the K-shell electron is ejected from the atom as photoelectron	9
Figure 2.3	The scenario of ejected electron	9
Figure 2.4	Photoelectric absorption coefficient of water and lead	11
Figure 2.5	The Compton scattering, in which in γ-ray interacts with an outer orbital electron of an absorber atom. Only a part of the photon energy is transferred to the electron, and the photon itself scattered at an angel	13
Figure 2.6	Schematic figure of pair production. Nuclear pair production in the coulomb field of the absorber nucleons	14
Figure 2.7	The origin of the K_α, K_β, L_α and L_β characteristic X-rays	16
Figure 2.8	The curve labeled Good Resolution illustrates one possible distribution around an average and the curve labeled Poor Resolution illustrates the response if a detector with inferior performance.	18
Figure 2.9	The formal energy resolution from single peak. FWHM is at the half maximum of the peak height	19
Figure 3.1	The Chemical Structure of PLA	30
Figure 3.2	Biodegradable polymers classification	32
Figure 3.3	(A) *Rhizophora spp*. tree trunk. (B) *Rhizophora spp.* chips. (C,D) Wood particles in different sizes	33
Figure 3.4	The sequence of operations involved in the fabrication of particle board from *Rhizophora spp*. wood.	39
Figure 3.5	Test apparatus for the internal bond (IB) strength	42
Figure 3.6	Field emission scanning electron microscope (FESEM) for studying the physical and morphological structure of samples.	44

Figure 3.7	LEGe Detector	46
Figure 3.8	Typical dipstick cryostat cross section	47
Figure 3.9	An illustration of the experiment set up	53
Figure 4.1	Density of fabricated bioplastic *Rhizophora spp*. particle board.	57
Figure 4.2	maximum load for bioplastic particleboard with 10% PLA	59
Figure 4.3	Average internal bond strength values of the bioplastic *Rhizophora spp*. particle board.	59
Figure 4.4	Comparison of internal bond strength for present study and other studies. Sample (A, B and C) *Rhizophora spp*. binderless particleboard each sample has different particle size of 147-74µm, 74-50 µm and <50 µm, respectively (Marashdeh *et al.*, 2011). Sample (D, E, F) bioplastic *Rhizophora spp*. particleboard each sample has different percentage of resin 6%, 8%, 10% PLA respectively (present study)	60
Figure 4.5	Thickness swelling (TS) and water absorption (WA) of bioplastic *Rhizophora spp*. particleboards.	62
Figure 4.6	A planar FESEM micrograph of 10% bioplastic *Rhizophora spp*. particleboard with the magnification of 100 x.	63
Figure 4.7	Micrographs of interaction of 10% PLA adhesive and *Rhizophora spp.* particles at a high magnified FESEM (5,000 x)	64
Figure 4.8	Energy calibration curve for LEGe detector using ^{241}Am and shows the relation between energy and channel number.	65
Figure 4.9	Channel number versus energy (keV) for pure metal plates	67
Figure 4.10	Mass attenuation coefficient at different K_α XRF peak energies of aluminum at different XRF beam energies compared with calculated XCOM for aluminum.	68
Figure 4.11	Mass attenuation coefficient at different K_α XRF peak energies of fabricated bioplastic *Rhizophora spp*. particleboard with different percentage adhesive at different energies.	70
Figure 4.12	Mass attenuation coefficient at different K_β XRF peak energies of fabricated bioplastic *Rhizophora spp*. particleboard with different percentage adhesive at different e energies.	70

Figure 4.13 Mass attenuation coefficient at different k_α energies for bioplastic *Rhizophora spp.* samples compared with calculated XCOM for Breast1, Breast 2 and Breast 3. 71

Figure 4.14 The percentage deviation of the mass attenuation coefficient of bioplastic *Rhizophora spp.* particleboard samples from the calculated Breast 2 (XCOM). 74

Figure 4.15 Comparison of the mass attenuation coefficient of bioplastic Rhizophora spp. particleboard with 10% pla at different energy with raw wood of *Rhizophora spp*. sample by Shakhreet *et al*. (2009), binderless *Rhizophora spp.* particleboard made by Marshadeh *et al*. (2012) and calculated XCOM for Breast1 and Breast 2. 75

LIST OF APPENDICES

Appendix A	Particleboard of *Rhizophora spp*. Wood Chip with Different Percentage Resin	86
Appendix B	Measurement of Length, Thickness, Width, Mass and Density of Fabricated *Rhizophora spp*. Particleboard	88
Appendix C	Maestro Software Personal Computer (PC)	90
Appendix D	Information of Metal	91
Appendix E	Linear and Mass Attenuation Coefficients of Fabricated Bio plastic *Rhizophora spp*. particleboard at different energy	92
Appendix F	Graphs of Linear Attenuation Coefficients of fabricated bio Plastic *Rhizophora spp*. Particleboard at Different Energy	102
Appendix G	Measurement of Water Absorption (WA) and Thickness Swelling (TS) of Fabricated *Rhizophora spp*. Particleboard	112
Appendix H	The χ^2 – test of Mass Attenuation Coefficient of Bioplastic *Rhizophora spp*. Particleboards Samples to XCOM Calculated Breast 1.	113
Appendix I	The χ^2 – test of Mass Attenuation Coefficient of Bioplastic *Rhizophora spp*. Particleboards Samples to XCOM Calculated Breast 2.	114
Appendix J	The χ^2 – test of Mass Attenuation Coefficient of Bioplastic *Rhizophora spp*. Particleboards Samples to XCOM Calculated Breast 3.	115

LIST OF SYMBOLS AND ABBREVIATIONS

α	Alpha
$\sigma_{\mu/\rho}$	Error in the mass attenuation coefficient (μ/ρ)
μ	Linear attenuation coefficient.
μ/ρ	Mass attenuation coefficient
Aw	Air weight of sample
CT	Computed tomography
dm	Unit of mass
E	Electron energy
E_b	Binding energy of electron
FE-SEM	Field emission scanning electron microscopy
FWHM	Full Width Half Maximum
g / cm^3	Gram per cubic centimeter
hν	Energy of photon
hν′	Energy of scattered photon
I	Intensity
IB	Internal Bond
JIS	Japanese Industrial Standard
keV	Kilo electron volt
L	Length
LEGe	Low Energy Germanium
Max	Maximum
MC	Moisture Content
MCA	Multichannel analyzer
MeV	Mega electron volt
MeV	Mega electron volt
min	Minimum
MPa	Mega Pascal

N	Number of incident photon
Ow	Dried weight of sample
P	Maximum failure load
P.b.	Particleboard
P.b. 10%	Particleboard with 10 % of PLA resin
P.b. 8%	Particleboard with 8 % of PLA resin
P.b. 6%	Particleboard with 6 % of PLA resin
PE	Polyethylene
PET	Polyethylene terephthalate
PHA	Pulse-height analyzer
PLA	Poly Lactic Acid
R	Resolution
R^2	Linear regression coefficient
s	Second
t	Thickness of disk
TS	Thickness swelling
V	Volume
WA	Water absorption
XCOM	X-ray computed
XRF	X-ray fluorescence
Z	Atomic number
β	Beta
γ	Gamma
θ	Compton electron angle
λ	Wavelength
ρ	Density
σ_c / ρ	Attenuation coefficients for Compton scattering
σ_{coh}	Attenuation coefficients for coherent scattering

τ / ρ	Attenuation coefficients for photoelectric effect
Φ	Scattering photon angle
χ^2	Chi-Square test (Statistical test)
$Л / \rho$	Attenuation coefficients for pair production

FABRIKASI DAN PEKALI ATENUASI JISIM PAPAN SERPAI BIO PLASTIK *RHIZOPHORA SPP.*

ABSTRAK

Papan zarah Bio plastik *Rhizophora spp*. telah fabrikasi dengan tahap rawatan resin asid polilaktik (PLA) yang berbeza sebanyak 6%, 8% dan 10% dengan ketumpatan sasaran 1 g/cm^3. Papan serpai Bio plastik *Rhizophora spp*. terhasiltelah diuji untuk sifat-sifat fizikal dan mekanikal. Morfologi permukaan papan serpai yang dihasilkan diperhatikan menggunakan kaedah Mikroskopi Imbasan Elektron Pancaran Medan (FESEM). Hasil kajian menunjukkan bahawa sampel yang dihasilkan dari *Rhizophora spp*. pada tahap rawatan 8% dan 10% resin asid polilaktik (PLA) mempamerkan kekuatan ikatan dalaman (IB) tertinggi dan mematuhi Piawaian Industri Jepun (JIS A-5908), manakala pada 6% resin asid polilaktik (PLA) tidak mematuhi piawaian tersebut Dari segi ciri-ciri fizikal, penyerapan air (WA) dan pembengkakan ketebalan (TS), keputusan papan serpai Bio plastik Rhizophora spp. pada 6%, 8% dan 10% resin asid polilaktik (PLA) mematuhi piawaian berkenaan. Pekali atenuasi jisim papan serpai direka telah ditentukan dengan menggunakan sinar-X pendarfluor (XRF) yang dipancarkan dari plat-plat logam tulen. Bahan-bahan yang digunakan untuk susunatur ujikaji ialah satu sumber Am-241 (^{241}Am) dengan keaktifan nominal 100 mCi, pengesan tenaga rendah Germanium (LEGe) dan lima plat logam tulen, iaitu Niobium (Nb), Molibdenum (Mo), Palladium (Pd), Perak (Ag) dan Timah (Sn). Tenaga XRF yang dipancarkan dari plat-plat logam itu adalah dalam julat 16.59 keV-25.26 keV. Hasil kajian menunjukkan bahawa pekali atenuasi jisim papan serpai bio plastik *Rhizophora spp*. didapati lebih hampir kepada nilai penghitungan XCOM bagi payudara dewasa.

FABRICATION AND MASS ATTENUATION COEFFICIENT OF BIOPLASTIC *RHIZOPHORA SPP. PARTICLEBOARD*

ABSTRACT

Bioplastic *Rhizophora spp.* particleboard was fabricated with different treatment levels of 6%, 8% and 10% from polylactic acid (PLA) resin with target density 1 g/cm^3. Particleboards produced were tested for the physical and mechanical properties. The surface morphology of the manufactured particleboard was viewed using Field Emission Scanning Electron Microcopy (FESEM). The results showed that samples produced from *Rhizophora spp.* at 8% and 10 % treatment level of PLA resin exhibited the highest internal bond (IB) strength and met Japanese Industrial Standards (JIS A-5908), while the 6% PLA sample did not fulfill the standard. In terms of physical characteristics water absorption (WA) and thickness swelling (TS), particleboard of 6%, 8 % and 10 % of PLA resin met the standard. The mass attenuation coefficients of the fabricated particleboards were determined by using X-ray fluorescence (XRF) emanating from pure metal plates. Materials used for the experimental set up were an Am-241 (^{241}Am) source with a nominal activity of 100 mCi, low energy Germanium (LEGe) detector and 5 metal plates; they are Niobium (Nb), Molybdenum (Mo), Palladium (Pd), Silver (Ag) and Tin (Sn). The energy of the XRF emitted from those metal plates ranged from 16.59 keV– 25.26 keV. The experimental value of the mass attenuation coefficient of the particleboards and the calculated XCOM values for the middle-age breast group are comparable. However, there was no influence on the attenuation properties of the particleboard of PLA resin contents. Taken together, these results strongly suggest that bioplastic *Rhizophora spp.* particleboard has the potential of acting as a phantom material at diagnostic photon energy.

CHAPTER 1

Introduction

1.1 Background

Determination of dosimetric characteristics of radiation beam is vital so that most appropriate set of treatment planning parameters is chosen. In diagnostic radiology, quality of a radiation beam is most usefully expressed in terms of its penetrating power, which is a function mainly of the mean photon energy (Kato *et al.*, 2004). Data on dose distribution are almost entirely derived from measurements in phantoms, and then are used in a dose calculation system devised to dose distribution in an actual patient (Khan, 1994). This data is actually representing different physics characteristics of the machine, beam and its energies in the form of dosimetric quantities.

The mass attenuation coefficient, the effective atomic number and the electron density are basic quantities vitally needed in order to the penetration of X-ray and photons in matter (Gowda *et al.,* 2004; Kucuk *et al.,* 2012). Mass attenuation coefficients are additionally required as a function of photon energy and material atomic number in a number of situations, for instance in diagnostic radiology, biological and other materials are of significant interest in industrial, agricultural and medical applications. Accurate values of photon mass attenuation coefficients are needed to establish the regions of validity of theory-based parameterization, in addition to providing essential data in diverse fields such as tomography, X-ray fluorescence studies and radiation biophysics. Besides, mass attenuation coefficients

are valuable in a number of applied fields including diagnostic radiology, nuclear diagnostic, radiation protection, nuclear medicine and radiation dosimetry (Baltas *et al.,* 2007; Bradley *et al.,* 1986). In order to properly choose the material for diagnostic radiology and radiation dosimetry, the features of the various materials must be fully recognized (Amutha and Ramprasath, 1999; Shivaramu and Ramprasath, 2000).

The coefficients are key parameters in investigating the interaction of radiation with matter that gives the fraction of energy scattered or absorbed. Mass attenuation coefficients, as known, depend on the photon energy and material's density (Baltas *et al.,* 2007). Also, the scattering and absorption of X-ray radiations are related to the density and effective atomic number of the material. The effective atomic number and the electron density of a composite material are considered as useful parameters in the dosimetric calculation of radiation dose in radiology and other field (Pawar *et al.,* 2012).

1.2 Statement of Problems

For clinical testing of diagnostic radiology, the tissue mimicking material for a phantom must have the same range of attenuation coefficient, radiation absorption and backscatter, as the organ they aim to mimic. At present, water is the primary phantom medium recommended for dosimetry, its measurements closely approximate the values of radiation absorption and scattering obtained for muscle and other soft tissues. Solid homogeneous phantoms have gained significant

popularity, especially for clinical dosimetry since it is not always practical to carry out dosimetric measurement in a water phantom (Khan, 1994).

However, many of the so-called tissue equivalent materials cannot provide good simulation to water at both low and high energies. Attenuation studies on *Rhizophora spp.* wood are also found to provide close agreement with attenuation results for water (Bradley *et al.,* 1991). However, *Rhizophora spp.* wood possesses some disadvantages if it were used as a phantom material: the raw wood has the tendency to crack and warp with time and there is difficulty in controlling the uniformity of properties throughout the plank or slab (Marshadeh *et al.,* 2011). Thus, it is crucial to fabricate a *Rhizophora spp*. particleboard phantom. The wood should be reduced into small particles and compressed into particleboards.

1.3 Objectives of Research

The objectives of this research are as follows:

1. To fabricate bioplastic *Rhizophora spp.* wood particleboard with a target density of 1.0 g /cm^3 by using polylactic acid (PLA) resin at different treatment levels of 6%, 8% and 10%.
2. To characterize the mechanical and physical properties of the fabricated bioplastic *Rhizophora spp.* particleboard made from different treatment levels of PLA.
3. To determine the mass attenuation coefficients of the bioplastic *Rhizophora spp*. particleboards at the photon energy range of 16.59 keV to 25.26 keV, and to compare them with calculated XCOM values of breast tissues.

1.4 Scope of Research

The scope of research is fabricating the bioplastic *Rhizophora spp.* particleboard that can be utilized in diagnostic photon energy range. The particleboards, to be fabricated, should match the human body characteristic such as the attenuation coefficient. The experiment was done by using different target elements in order to determine the mass attenuation coefficient. The bioplastic *Rhizophora spp.* particleboard phantom with different percentages of polylactic acid were used to see the differences of mass attenuation coefficients. In this study X-ray fluorescence (XRF) was used to produce monoenergetic photon at various energies.

1.5 Outline of the Thesis

This thesis presents a description of a fabricated bioplastic *Rhizophora spp.* particleboard phantom to be used in radiation dosimetry in diagnostic radiology. In Chapter 1, the background for the diagnostic radiology and mass attenuation, statement of problems, objectives and scope of the thesis are described. Chapter 2 reviews the theory of radiation and a brief literature review of previous studies and the fabrication of radio dosimetric phantoms. Chapter 3 presents the methodology of the research, including the materials and methods for fabricating the particleboard phantom, the set-up of the experiment and the laboratorial measurements. The results and discussion are mentioned in Chapter 4. In the last chapter there are conclusions and recommendations for future work.

CHAPTER 2

Literature Review and Theory

2.1 Linear Attenuation Coefficient

A narrow beam of monoenergetic photon is incident on an absorber of variable thickness. A detector is put at a fixed distance from the source and sufficiently farther away from the absorber so that only the primary (those photons that passed through the absorber without interacting) are measured in this arrangement. Thus, if a photon interacts with an atom, it is either completely absorbed or scatter away from the detector (Beutel and Kundel, 2000; Demir and Tursucu, 2012).

The amount of deducted photons (dN) is proportional to the number of incident photons (N) and to the thickness of absorber (dx). Mathematically,

$$dN \alpha N\, dx \tag{2.1}$$

$$dN = -\mu N\, dx \tag{2.2}$$

where μ is the constant of proportionality, called the attenuation coefficient. The minus sign indicated that the number of photons decreases as the absorber thickness increases. The above equation can also be written in terms of intensity (I):

$$dI = -\mu I\, dx \tag{2.3}$$

If thickness x is expressed as a length, then μ is called the linear attenuation coefficient (Sethi, 2006).

The differential equation for attenuation can be solved to yield the following equation:

$$I(x) = I_0 e^{-\mu x} \tag{2.4}$$

where $I(x)$ is the intensity transmitted by a thickness x and I_0 is the intensity incident on the absorber. If $I(x)$ is plotted as a function of x for a narrow monoenergetic beam, a straight line will be obtained on a semi logarithmic paper, showing that the attenuation of a monoenergetic beam is described by an exponential function (Khan, 1994; Gurler and Tarim, 2012)

2.2 Mass Attenuation Coefficient

In general, this coefficient depends on the energy of photon and the type of material. Since the attenuation produced by a thickness x depends on the number of electrons presented in that thickness, μ depends on the density of the material. Thus, by dividing μ by density ρ, the resulting coefficient (μ/ρ) will be independent of density; μ/ρ is known as the mass attenuation coefficient. Since, the density has been factored out and its dependence on the nature of the material does not involve density but rather the atomic composition (Tsechanski, 2006; Sethi, 2006; Demir, 2012)

2.3 Interactions of Photons with Matter

Four main types of interactions participate in attenuation of a photon by absorbing materials, such as coherent scattering, photoelectric effect, Compton Effect, and pair production. Every process possesses its own attenuation coefficient that varies with photon's energy and absorbing material's atomic number. (Choppin *et al.*, 2002 ; Tsechanski, 2006). The total attenuation coefficient is the sum of individual coefficients for these processes:

$$\mu/\rho = \sigma_{coh}/\rho + \tau/\rho + \sigma_c/\rho + \pi/\rho \quad (2.5)$$

where σ_{coh}, τ, σ_c, π are attenuation coefficients for coherent scattering, photoelectric effect, Compton Effect and pair production respectively.

2.3.1 Coherent Scattering

The coherent scattering which is also known as classical scattering or Rayleigh scattering, is shown in Figure 2.1. This process can be visualized by taking the wave nature of electromagnetic radiation into consideration. This interaction consists of an electromagnetic wave passing near the electron and setting it into oscillation. The oscillating electron reradiates the energy at the same frequency as the incident electromagnetic wave. This scattered X-ray has the same wavelength $(\lambda = \lambda')$ as the incident beam. Thus no energy is changed into electronic motion and no energy is absorbed in the medium. The only effect is the scattering of the photon at small angles. The coherent scattering is probable in high atomic number materials

and with photons of low energy. The process is only of academic interest in radiation therapy (Khan, 1994).

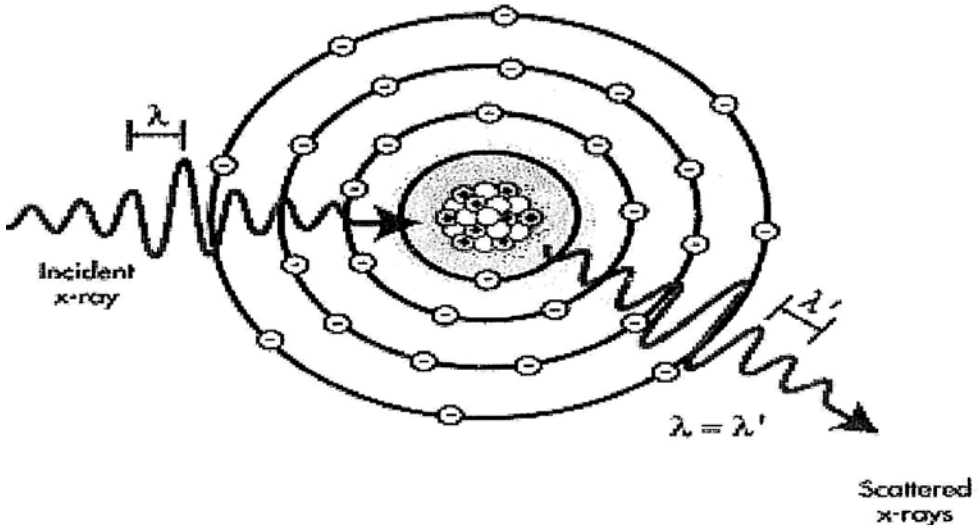

Figure 2.1. Coherent scattering. A photon with energy *hv* interacts with a K-shell electron. This scattered X-ray has the same wavelength ($\lambda = \lambda'$) as the incident beam (Bushberg *et al.,* 2002).

2.3.2 Photoelectric Effect

The photoelectric effect is a phenomenon in which a photon interacts with an atom and ejects one of the orbital electrons from the atom as shown in Figure 2.2. In this process, the entire energy *hv* of the photon is first absorbed by the atom and then transferred to the atomic electron.

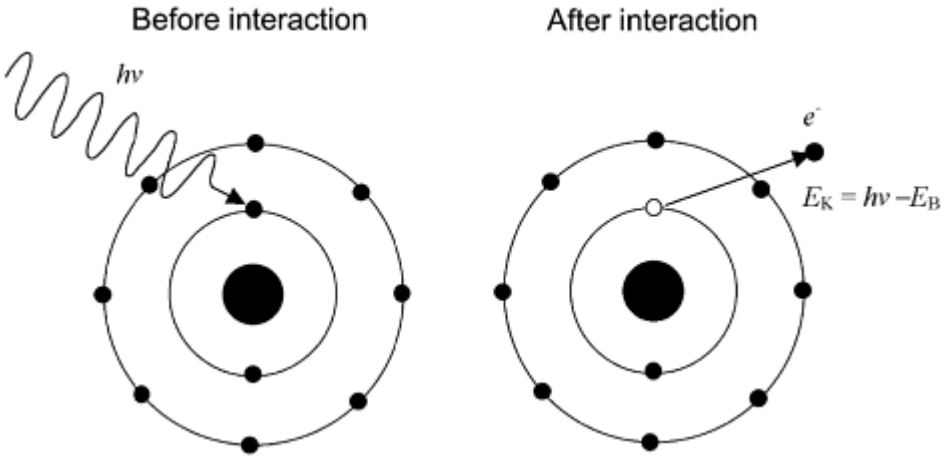

Figure 2.2. Schematic diagram of photoelectric effect. A photon with energy *hv* interacts with a K-shell electron. The photon is absorbed completely and the K-shell electron is ejected from the atom as photoelectron (Podgorsak, 2005).

The kinetic energy of the ejected electron is equal to $hv - E_b$, where E_b is the binding energy of the electron. Interaction of this type can take place with electrons within the K, L, M or N shells (Sethi, 2006) as can be seen in Figure 2.3.

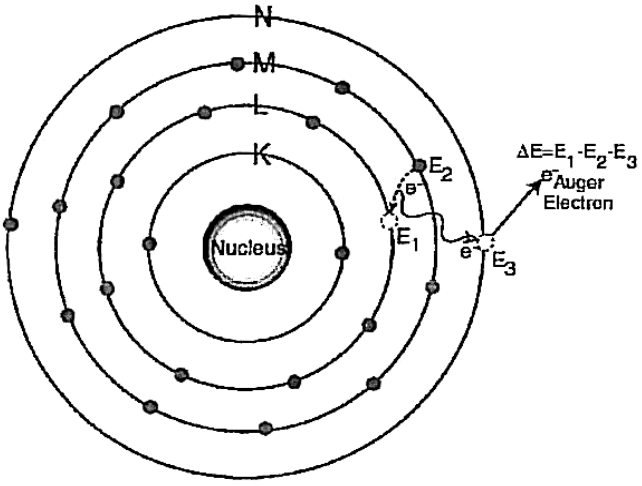

Figure 2.3. The scenario of ejected electron.

After the electron has been ejected from the atom, a vacancy is created in the shell, thus leaving the atom in excited state. The vacancy can be filled by an outer orbital electron with the emission of characteristic X-ray. There is also the possibility of emission of auger electrons, which are monoenergetic electrons produced by the absorption of characteristic X-ray internally by the atom. Since the *K* shell binding energy of soft tissue is only about 0.5 keV, the energy of the characteristic photons produced in biologic absorbers is very low and can be considered to be locally absorbed. For higher-energy photons and higher atomic number materials, the characteristic photons are of higher energy and may deposit energy at large distances compares with the range of the photoelectron. In such cases, the local energy absorption is reduced by the energy emitted as characteristic radiation which is considered to be remotely absorbed (Boone, 2000).

The probability of photoelectric absorption depends on the photon energy as illustrated in Figure 2.4, where the mass photoelectric attenuation coefficient (τ/ρ) is plotted as a function of photon energy. Data are shown for water, representing a low atomic number material similar to tissue and for lead, representing a high atomic number material. On logarithmic paper, the graph is almost a straight line with a slope of approximately -3; therefore, the relationship between τ/ρ and photon energy is:

$$\tau/\rho \; \alpha \; 1/E^3 \qquad (2.6)$$

The Figure 2.4 for lead has discontinuities at about 15 and 88 keV. These are called absorption edges and correspond to the binding energies of *L* and *K* shells. A photon with energy less than 15 keV does not have enough energy to eject an *L* electron (Hendee and Ritenour, 2003). When the photon has an energy that just

equals the binding energy of the L shell electrons, resonance occurs and the probability of photoelectric absorption involving the L shell becomes very high. Beyond this point, if the photon energy is increased, the probability of photoelectric attenuation decreases approximately as $1/E^3$ until the next discontinuity, the K absorption edge (Sethi, 2006). At this point on the graph, the photon has 88 keV energy, which is just enough to eject the K electron. As seen in Figure 2.4, the absorption probability in lead at this critical energy increases dramatically, by a factor of about 10.

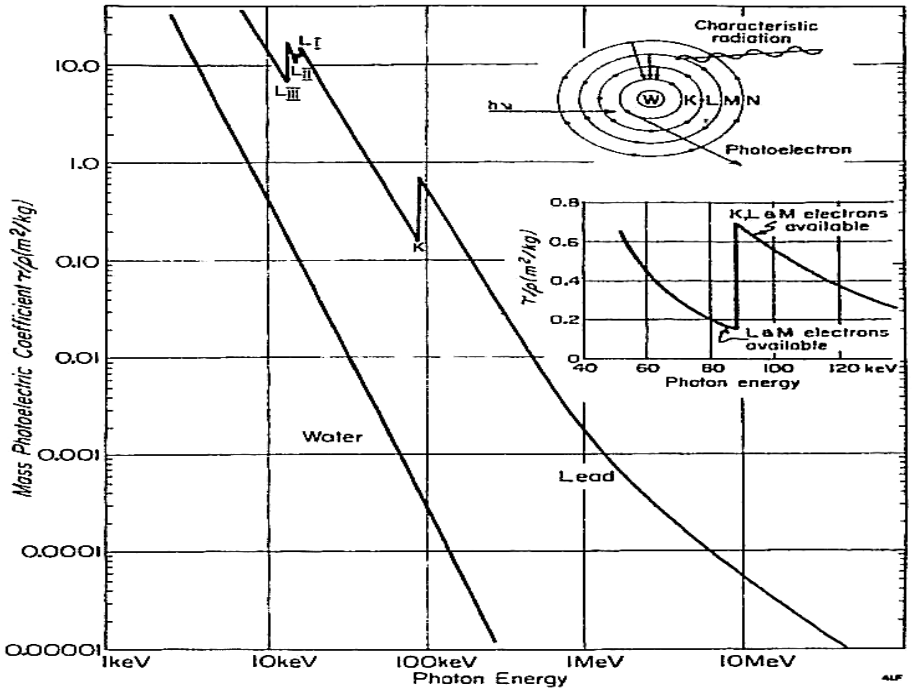

Figure 2.4. Photoelectric absorption coefficient of water and lead (Khan, 1994).

The discontinuities or absorption edges for water are not shown in the Figure 2.4 because the K absorption edge for water occurs at very low photon energies (˜≈ 0.5 keV). The data for various materials indicate that photoelectric attenuation

depends strongly on the atomic number of the absorbing material (Brown *et al.*, 2008). The following approximate relationship holds:

$$\tau/\rho \; \alpha \; Z^3 \tag{2.7}$$

This relationship forms the basis of many applications in diagnostic radiology. The difference in Z of various tissues such as bone, muscle and fat amplifies difference in x-ray absorption, provided the primary mode of interaction is photoelectric. This Z^3 dependence is also exploited when using contrast materials such as $BaSO_4$ mix and Hypaque. In therapeutic radiology, the low energy beams produced by superficial and orthovoltage machines cause unnecessary high absorption of X-ray energy in bone as a result of this Z^3 dependence.

The angular distribution of electrons emitted in a photoelectric process depends on the photon energy. For a low energy photon, the photoelectron is emitted most likely at 90 degrees relative to the direction of the incident photon. As the photon energy increases, the photoelectrons are emitted in more forward direction (Sethi, 2006).

2.3.3 Compton Scattering

The Compton process is illustrated in Figure 2.5, the photon interacts with an atomic electron as though it were a free electron. The term frees here means that the binding energy of the electron is much less than the energy of the bombarding photon. In this interaction, the electron receives some energy from the photon and is

emitted at an angle θ. The photon, with reduced energy, is scattered at angel Ø (Janssens, 2005).

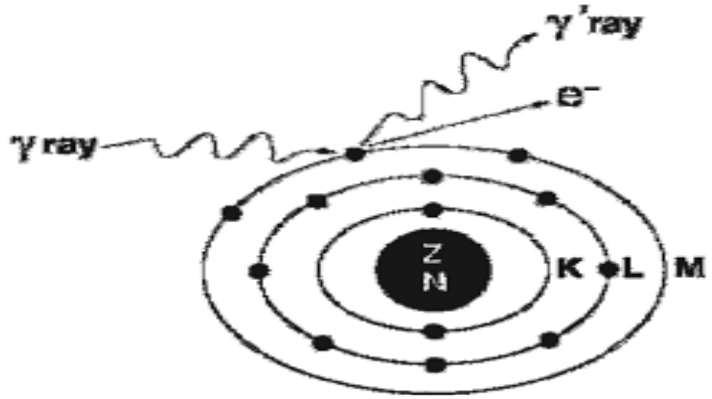

Figure 2.5. The Compton scattering, in which in γ-ray interacts with an outer orbital electron of an absorber atom. Only a part of the photon energy is transferred to the electron, and the photon itself scattered at an angel (Saha, 2006)

The Compton process can be analyzed in terms of a collision between two particles, a photon and an electron. By applying the laws of conservation of energy and momentum, one can derive the following relationships:

$$E = h\nu_0 \frac{\alpha(1-\cos\phi)}{1+\alpha(1-\cos\phi)} \tag{2.8}$$

$$h\nu' = h\nu_0 \frac{1}{1+\alpha(1-\cos\phi)} \tag{2.9}$$

$$\cos\theta = (1+\alpha)\tan\phi/2 \tag{2.10}$$

where $h\nu_0$, $h\nu'$ and E are the energies of the incident photon, scattered photon and electron, respectively and $\alpha = h\nu_0 / m_0 c^2$, where $m_o c^2$ is the rest energy of the electron (0.511 MeV). If $h\nu_o$ is expressed in MeV, then $\alpha = h\nu_o / 0.511$ (Sakurai *et al.*, 1995).

2.3.4 Pair Production

If the energy of the photon is more than 1.02 MeV, the photon can probably interact with matter through the mechanism of pair production as shown in Figure 2.6. In this process, the photon interacts strongly with the electromagnetic field of an atomic nucleus and gives up all its energy in the process of creating a pair consisting of a negative electron (e^-) and a positive electron (e^+). Since the rest mass energy of the electron is equivalent to 0.51MeV, a minimum energy of 1.02 MeV is needed to create the pair of electrons (Sethi, 2006; Choppin *et al.*, 2002). The photon energy in excess of this threshold is shared between the particles as kinetic energy. The total kinetic energy available for the electron-positron pair is given by *(hv-1.02*) MeV. The particles tend to be emitted in the forward direction relative to the incident photon (Kamal, 2010).

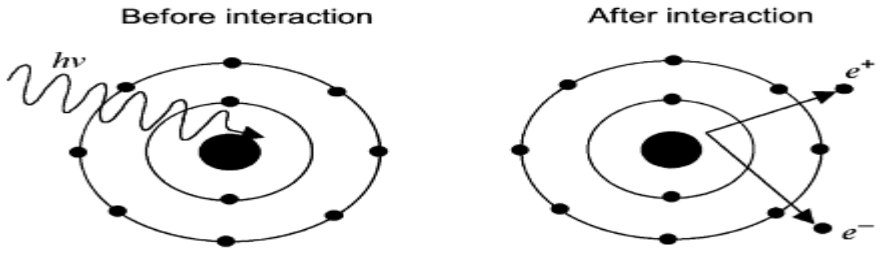

Figure 2.6. Schematic figure of pair production. Nuclear pair production in the coulomb field of the absorber nucleons (Podgorsak, 2005)

2.4 X-ray Fluorescence

The process of emissions of characteristic X-ray by filling the vacancy inner shell from an out shell electrons called X-ray Fluorescent or XRF. The term fluorescence is applied to phenomena in which the absorption of higher energy radiation results in the re-emission if lower energy of radiation.

Instead of ionizing process, excitation process also can occur if the energy of the incoming radiation is only equal or slightly higher than the electron binding energy. Therefore, the electron gets enough energy to move to the higher energy levels. The atom is said to be in the excited state. This situation only occurs for a short period of time and the electron will return to the ground state naturally. Thus, it will emit a characteristic X-ray as return to the lower energy level (Janssens, 2005).

For an atom in an excited state, the ejection of an auger electron is a competitive process to the emission of the characteristic X-ray. Sometimes, as the atom returns to its stable condition, instead of emitting a characteristic X-ray, it transfers the excitation energy directly to one of the outer electrons, causing it to be ejected from the atom. The ejected electron is known as auger electron. Auger electrons are more probable in the low Z elements than in high *Z* elements. The characteristic X-ray is labeled as *K, L, M* or *N* to denote the shell they created from. Another designation alpha (α), beta (β) or gamma (γ) is made to mark the X-rays that originated from the transitions of electrons from higher shells. Hence, a K_α X-ray is produced from a transition of an electron from *L* to *K* shell and K_β X-ray is produced from a transition of electron from *M* to *K* shell, etc. since within the shells there are multiple orbits of higher and lower binding energy electrons, a further designation is

made as *α1, α2* or *β1, β2*, etc. to denote transitions of electrons from these orbits into the same lower shell (Boone, 2000) as can be seen in Figure 2.7.

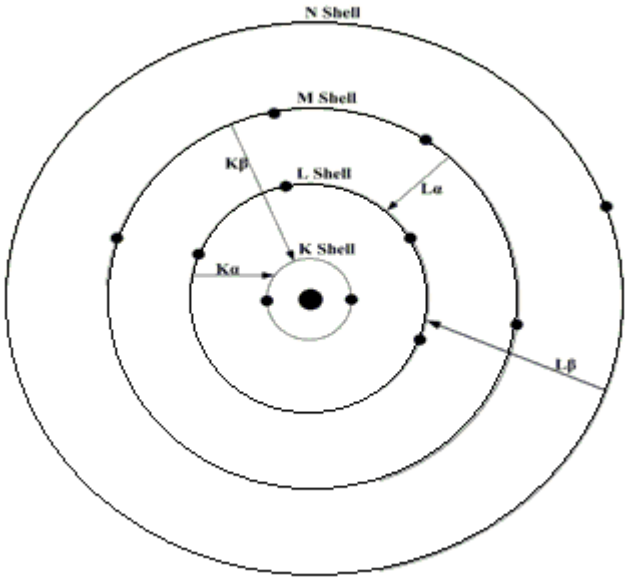

Figure 2.7. The origin of the K_α, K_β, L_α and L_β characteristic X-rays (Cember, 2008)

2.4.1 Sources of X-ray Fluorescence (XRF)

There are several numbers of physical processes that can lead to the population of the excited atomic state which X-ray fluorescence originated. Generally, relative yield of *K*, *L* and subsequent series will depend on the excitation method. However, the energy of the characteristic photon is fixed by the atomic binding energies. There are two ways that are practically importance for compact laboratory sources of fluorescence X-ray; excitation by radioactive decay and excitation by external radiation.

For the excitation by radioactive decay, two nuclear decay processes were contributed in the production of X-ray fluorescence photons. Those two processes are internal conversion and electron capture that will create a vacancy in the electron orbital. When the vacancy is subsequently filled, X-rays emitted are characteristic of the product element.

X-ray fluorescence (XRF) also can be produced by excitation from external radiation. X-ray or gamma rays can be used as the external radiation. When gamma ray or X-ray from a source radiation strikes on the target material, it will create excited or ionized atoms in the target. The energy of XRF emitted depends on the target material. Target with low atomic number will result in soft characteristic X-rays while high *Z* number target produce harder and higher energy of characteristic X-rays. The energy of incident radiation must overcome the binding energy in which maximum XRF energy expected from the target (Han, 2009a).

2.5 Pulse Height Analyzers

When an energy-sensitive detector is used, the amplitude of the voltage pulse from the amplifier is proportional to the amount of energy deposited in the detector by the detected radiation event. By examining the amplitudes of the amplifier of the amplifier output pulses, it is possible to determine the energies of detected radiation events. A device used for this purpose is called a pulse-height analyzer (PHA) (Cherry *et al.,* 2012). A PHA is used to select for those pulses from the amplifier falling with selected voltage amplitude intervals or called "channels". A device that is capable of analyzing simultaneously within many different intervals or channels is

called a multichannel analyzer (MCA). A pulse-height spectrum is a display showing number of events detected (count) versus the amplitude of those events (Knoll, 2000).

2.6 Energy Resolution

In many application of radiation detector, the objective is to measure the energy distribution of the incident radiation. These effects are classified under the general term radiation spectroscopy (Celiktas *et al.*, 2012).One important property of detector in radiation spectroscopy can be examined by noting its response to a monoenergetic source of that radiation pulse height H_0. Figure 2.8 illustrates the differential pulse height distribution that might be produced by a detector under these conditions. This distribution is called respond function of the detector for the energy used in the determination. The curve labeled good resolution illustrates one possible distribution around an average. The second curve, labeled poor resolution illustrates the response of a detector with inferior performance.

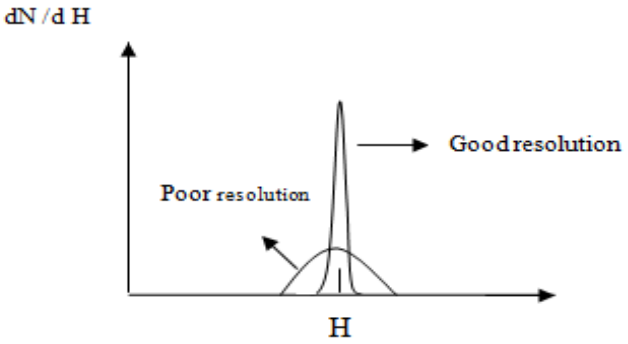

Figure 2.8. The curve labeled good resolution illustrates one possible distribution around an average and the curve labeled poor resolution illustrates the response if a detector with inferior performance (Knoll, 2000).

The same numbers of pulses are recorded in both cases and the areas under each peak are equal. The width reflects the fact that a large amount of fluctuation was recorded from pulse to pulse even though the same energy was deposited in the detector for each event (Knoll, 2000). If the amount of these fluctuations is made smaller, the width of the corresponding distribution will also become smaller and the peak will approach a sharp spike or a mathematical delta function. The ability of a given measurement to resolve fine detail in the incident energy of the radiation is obviously improved as the width of the response become smaller and smaller. A formal definition of detector energy resolution is shown Figure 2.9.

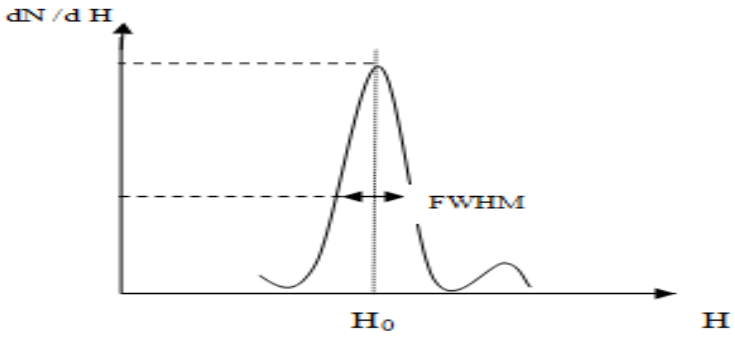

Figure 2.9. The formal energy resolution from a single peak. FWHM is at the half maximum of the peak height.

The differential pulse height distribution for a hypothetical detector is shown under the same assumption that only radiation of a single energy is being recorded. The full width at half maximum (FWHM) is illustrated in the figure and is defined as the width of the distribution at a level at is just half the maximum ordinate of the peak. Based on his definition, any background or continuum on which the peak may be superimposed is negligible or has been subtracted away. The energy resolution of

the detector is conventionally defined as the FWHM divided by the location of the peak centroid H_0. The energy resolution R is thus a dimensionless fraction conventionally expressed as a percentage. It should be clear that the smaller the figure for the energy resolution, the better the detector will be able to distinguish between two radiations whose energies lie near each other. Energy resolution become better (FWHM smaller) with increasing in gamma ray energy since the increasing of energy decrease the percentage statistical variation (Knoll, 2000).

There are a number of potential sources of fluctuation in the response of a given detector which results in imperfect energy resolution. These include any drift of the operating characteristics of the detectors during the course of measurements, source of random noise within the detector and instrumentation system, and statistical noise arising from the discrete nature of the measured signal itself (Knoll, 2000).

The third source is in some sense the most important because it represents an irreducible minimum amount of fluctuation that will always be present in the detector signal no matter how perfect the remainder of the system is made. In a wide story category of detector applications, the statistical noise represents the dominant source of fluctuation in the signal and thus sets an important limit on detector performance.

2.7 Error Analysis

The intensity of the beam detected was determined from the net counts under the peak of the XRF spectrum given by following equation.

$$S = (T\text{-}B) \pm \sqrt{T + B} = (T - B) \pm \sqrt{S + 2B} \quad (2.11)$$

Where T is the integral count under the peak and B is the associated background counts.

The maximum net counts under the peak is then

$$S_{max} = (T\text{-}B) + \sqrt{S + 2B} \quad (2.12)$$

and the minimum net counts possible is

$$S_{min} = (T\text{-}B) - \sqrt{S + 2B} \quad (2.13)$$

Then the maximum value of the linear attenuation coefficient is given by

$$\mu_{max} = x^{-1} \ln (S_{0\,max} / S_{min}) \quad (2.14)$$

and the minimum value of the linear attenuation coefficient is given by

$$\mu_{min} = x^{-1} \ln (S_{0\,min} / S_{max}) \quad (2.15)$$

where x is the thickness of the sample and S_0 is the counts in the unattenuated peak of the incident beam. The mean deviation from the best linear attenuation coefficient μ was calculated from $\sigma_\mu = \pm (\mu_{max} - \mu_{min}) / 2$. The error in the mass attenuation coefficient (μ/ρ) is then given by

$$\sigma_{(\mu/\rho)} = \left(\frac{\sigma\mu}{\mu} + \frac{\sigma\rho}{\rho} \right) \times (\mu/\rho) \quad (2.16)$$

where ρ is the density of the sample (Bauk and Tajuddin, 2008**)**.

2.8 Phantom

It is seldom possible to measure dose distribution directly in patients treated with radiation. Data on dose distribution are almost directly derived from measurement in phantom. Tissue equivalent materials are usually large enough in volume to provide full scatter condition for given beam. These basic pieces of data are used in a dose calculation system devised to predict dose distribution in an actual patient.

Ideally, the phantom material should be water-equivalent, so that it has the same absorption and scatter properties as water. Basic dose distribution data are usually measured in water phantom which closely approximates the radiation absorption and scattering properties of muscle and other soft tissue (Tuffour-Achampong *et al.,* 2012). Another major reason for the choice of water as a phantom material is that it is universally available with reproducible radiation properties. The element composition, nominal density and mean atomic number of some common phantom materials used as water substitute. Density for water is 1.00 g/cm^3.

A water phantom, however, poses some practical problems when using in conjunction with detectors which are affected by water unless they are designed to be waterproof. In most cases, the detector is encased in a thin plastic (water equivalent) sleeve before immersion into the water phantom. Since it is not always possible to put radiation detectors in water, solid dry phantom have been developed as substitutes for water. Ideally, for a given materials to be tissue or water equivalent, it

must have the same effective atomic number, number of electron per gram, mass density and attenuation coefficient.

The attenuation coefficients of various elements and compounds of dosimetric interest have been tabulated by a number of works (Hubbell, 1982; Berger and Seltzer, 1984). White (1977) formulated tissue substitutes for a wide range of applications for example dosimetric phantoms, radiographic test objects and dosimeter components, the material composition being derived for both photon and electron interactions.

Earlier theoretical evaluations of plastic phantoms with high energy X-rays applying scaling factors have shown to be comparable (Peschel and Schulz, 1974). Schulz and Nath (1980) investigated polystyrene and plastic phantoms using ^{137}Cs and ^{125}I gamma rays, finding the constant atomic compositions and electron densities to be suitable for their use as phantoms for high energy X-rays and electrons. Wong *et al.* (2001) investigated the absorbed dose calibration in polystyrene phantom and comparing the results with those for solid water phantom and found comparable results. However, before any solid phantom material is used as a water substitute, a comparison with measurements in water should carefully be performed (Tello *et al.*, 1995).

2.9 Study on Mangrove Wood *Rhizophora spp.* Phantom

Rhizophora spp. wood (tropical hard wood) is considered a strong wood and is suitable for structural applications. This wood is hard and heavy. They are

however some disadvantages of using the raw material of *Rhizophora spp*. in radiation dosimetry studies especially with regards to phantom design.

The disadvantages are:

a) The trunk diameter of *Rhizophora spp.* trees is limited where the maximum diameter which is available in around 28cm.
b) It is a hard wood and heavy to handle, so it is difficult to cut and shape it.
c) With long periods of time, the *Rhizophora spp*. chunks are observed to be cracked through the drying process.
d) Similarly, with long periods of time, the slabs of *Rhizophora spp*. tend to be curved or arched which causes unsymmetrical deformations in the slabs which may cause problems in the stacking of slabs.

To overcome the above disadvantages of raw (natural) *Rhizophora spp*. another way to modify this natural wood to be flexible for use as a phantom for radiation dosimetry has to be found. It is this reason that the focus in this work has been on fabricating particleboards of *Rhizophora spp.*

The efforts to develop particleboards have started since 1920's in the United States. In that time, failures in making particle boards were primary due to the lack of suitable adhesives. Successful particleboard making was started in 1930's where the development of new thermosetting resin had been found. Then in 1941, the first industrial production of particleboards using synthetic resin was started in Bremen, Germany. The importance of particleboard lies in the utilization of residue and low grade wood. Particleboards manufacturing are so flexible as it could be produced in the form of large panel sizes with a full range of thicknesses (Moslemi, 1974).